


Terahertz Lasing with Weak Plasmon Modes in Periodic Graphene Structures

Denis V. Fateev^{1,2,*}, Olga V. Polischuk¹, Konstantin V. Mashinsky¹, Ilya M. Moiseenko¹, Mikhail Yu. Morozov¹, and Viacheslav V. Popov¹

¹*Kotelnikov Institute of Radio Engineering and Electronics, Russian Academy of Sciences, Saratov 410019, Russia*

²*Saratov State University, Saratov 410012, Russia*

 (Received 7 December 2020; revised 5 February 2021; accepted 10 February 2021; published 15 March 2021)

The achievement of the laser regime upon the excitation of weak plasmon modes in structures based on active graphene has been theoretically investigated. The weak “acoustic” plasmon modes in two-layer structures and weak “nonradiative” gated modes in noncentrosymmetric grating-gated structures are investigated. The radiative damping and gain rate of strong and weak plasmon modes in graphene structures are calculated. The possibilities of changing the radiative damping of plasmon modes by changing the geometry of the structure are considered. It is proposed to use weak plasmon modes with low radiative damping for decreasing the threshold for the laser plasmon regime in periodic graphene structures.

DOI: [10.1103/PhysRevApplied.15.034043](https://doi.org/10.1103/PhysRevApplied.15.034043)

I. INTRODUCTION

Terahertz (THz) plasmons in two-dimensional materials have been studied for a long time [1]. Since the onset of the graphene boom [2], studies of THz plasmons have actively moved to a truly two-dimensional material, graphene [3–5]. Basically, the advantage of graphene plasmons is associated with the high mobility of electrons in high-quality graphene structures [6,7], which leads to the possibility of achieving a high Q factor of plasmon resonances in the THz frequency range [8]. An interesting feature is the electrically tunable doping of graphene [9,10], which leads not only to easy electrical tuning of the plasmon frequency, but also to the possibility of switching the type of carriers from electrons to holes. The nonlinear properties of plasma oscillations in graphene are used to create devices that rectify THz radiation [11,12].

A promising direction in the study of plasmons in graphene is the creation of amplifiers and generators of THz radiation at the plasma resonance [13–15]. A number of works are devoted to the active properties of graphene, in which the possibility of creating the carrier population inversion in graphene is investigated [16–18]. The possibility of amplifying THz radiation in a photonic cavity based on active graphene has been experimentally demonstrated [19]. Despite significant results in the field of obtaining the population inversion in graphene, many works are still devoted to solving the problems associated with the difficulties of creating a population inversion in graphene [20,21]. Studies on increasing the lifetime of

inverted carriers are mainly aimed at suppressing nonradiative Auger recombination and decreasing the recombination with the emission of optical phonons in graphene. For this purpose, it is proposed to pump graphene with injection cold [16] or cooled charges [22]. For transverse injection pumping, it is proposed to use material with a small band gap from which diffusion of electron-hole pairs occurs [23]. Longitudinal injection pumping from n - and p -doped graphene regions also looks promising [24]. Amplifying THz plasmons in hydrodynamic graphene is possible with a dc drift of charge carriers [25]. Based on the experimental data [26,27], the hydrodynamic regime in graphene can be achieved in the low part of the THz range, below the frequency of carrier-carrier collisions [28].

The most promising for plasmon excitation is using short-period coupling structures, since in this case the energy exchange between the THz electromagnetic wave and the plasmon occurs most effectively [29]. In such structures, the most useful factor that describes the efficiency of interaction between a plasmon and a THz wave is the radiative damping, which accounts for the decay of plasmon due to the emission of THz electromagnetic waves from the structure [30]. The most effective excitation of plasmons in periodic structures occurs under the condition of equality of the dissipative and radiation dampings of the plasmon [30]. For active plasmonic structures, it was found that the plasmonic laser regime occurs in a situation when the gain from the active medium compensates the dissipative and radiative dampings [31] together.

It was found that in spatially symmetric structures, plasmon modes with a large radiative damping are mainly excited. In noncentrosymmetric periodic structures, the excitation of weak “nonradiative” plasmon modes is also

*FateevDV@yandex.ru

possible [32]. The weak plasmon modes can be utilized for excitation of propagating plasmon in periodic graphene structures [33,34].

In this work, we investigate the appearance of a lasing regime of THz radiation with weak plasmon modes. Weak “nonradiative” plasmon modes in noncentrosymmetric grating-gate structure and weak “acoustic” plasmon modes in two-layer graphene structure are investigated. The influence of radiative damping on the amplification of THz radiation by weak plasmon modes is considered. The advantages of using weak modes for THz lasing are discussed.

II. OSCILLATOR MODEL FOR PLASMONS

Let us estimate the energy absorption of the incident electromagnetic wave using a planar periodic graphene plasmonic oscillator model. Since, for plasmon excitation in THz frequency range, the unit cell of a periodic structure is much smaller than the THz wavelength, this periodic structure can be considered as a spatially homogeneous two-dimensional plasmonic system described by effective parameters. The plasmon oscillations in such a linear oscillator model can be described by the equation

$$\frac{d^2x}{dt^2} + (\gamma_d + \gamma_g) \frac{dx}{dt} + \omega_{pn}^2 x = -\frac{e}{m_d} E_x, \quad (1)$$

where x is the space coordinate of the deviation of the carriers from equilibrium, ω_{pn} is the frequency of the n th plasmon mode, with $n = 1, 2, 3 \dots$, m_d is the dynamic mass of charge carriers in graphene [35], for small temperatures $m_d = \mathcal{E}_F/v_F^2$, e is the elementary charge, γ_d is the dissipative damping rate, γ_g is the gain rate for active graphene (plasmon oscillations are amplified for $\gamma_d + \gamma_g < 0$), and E_x is the acting electric field.

Calculating the total dipole moment of the plasmon mode using Eq. (1) in the vicinity of the resonance of the n th plasmon mode, the effective admittance of a thin plasmonic active layer in the model of a resonant surface layer can be written similarly to Ref. [30]

$$Y_{\text{eff}}(\omega) \approx Y_n(\omega) \approx -\frac{e^2 N_s}{m_d} \frac{\beta_n^2}{\gamma_d + \gamma_g + i(\omega - \omega_{pn})},$$

where $Y_n(\omega)$ is the admittance of the structure for the n th plasmon mode, N_s is the surface charge density in graphene, and β_n^2 is the coupling strength of the THz wave and the n th plasmon mode (β_n^2 can be considered as a fraction of charges participating in the n th mode of the plasmon oscillation).

This model can be used to estimate the transmission and reflection coefficients for the structure as

$$T_n(\omega) = T_0 \frac{(\omega - \omega_{pn})^2 + (\gamma_d + \gamma_g)^2}{(\omega - \omega_{pn})^2 + (\gamma_d + \gamma_g + \gamma_{rn})^2},$$

$$R_n(\omega) = R_0 \frac{(\omega - \omega_{pn})^2 + (\gamma_d + \gamma_g + \gamma_{rn}/\sqrt{R_0})^2}{(\omega - \omega_{pn})^2 + (\gamma_d + \gamma_g + \gamma_{rn})^2},$$

respectively, where

$$T_0 = \frac{4\sqrt{\varepsilon_t \varepsilon_b}}{(\sqrt{\varepsilon_t} + \sqrt{\varepsilon_b})^2}; \quad R_0 = \frac{(\sqrt{\varepsilon_t} - \sqrt{\varepsilon_b})^2}{(\sqrt{\varepsilon_t} + \sqrt{\varepsilon_b})^2},$$

with ε_t and ε_b being the dielectric constants of surrounding top and bottom media above and below the resonant layer, respectively. The value

$$\gamma_{rn} = \frac{e^2 N_s}{m_d} \frac{Z_0 \beta_n^2}{\sqrt{\varepsilon_t} + \sqrt{\varepsilon_b}} \quad (2)$$

describes the radiative damping of the n th plasmon mode in the resonant layer [30].

The sum of the reflection and transmission coefficients at the plasma resonance frequency can be written as

$$R_n(\omega_{pn}) + T_n(\omega_{pn}) = 1 - A_n(\omega_{pn}),$$

where

$$A_n(\omega_{pn}) \simeq \frac{2(\gamma_d + \gamma_g)\gamma_{rn}}{(\gamma_d + \gamma_g + \gamma_{rn})^2} (1 - \sqrt{R_0}). \quad (3)$$

is the absorption coefficient ($A < 0$ for the amplification regime). For active structures the sum of the reflection and transmission coefficients $R_n + T_n$ can be viewed as the *amplification* coefficient.

The THz radiation amplification regime is achieved when the sum of the reflection and transmission coefficients exceeds the unity. The lasing regime is reached under the condition when the denominator of Eq. (3) is equal to zero, $\gamma_d + \gamma_{rn} = -\gamma_g$, i.e., the laser generation of plasmons occurs when the dissipative and radiative losses are compensated by the gain (Fig. 1). Such a simple model of plasmon oscillator, Eq. (3), gives the following basic implications:

1. At zero plasmon radiative damping, there is no interaction between the wave and the structure, as a result of which plasmon modes with zero radiative damping are not excited.
2. For the emergence of an amplified plasmon mode, compensation of the dissipative losses by the gain is

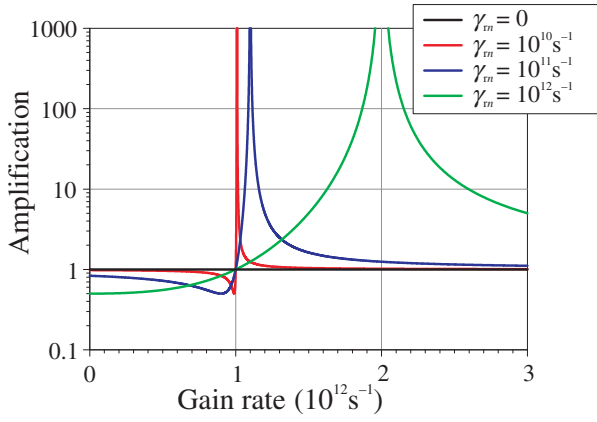


FIG. 1. Dependence of the amplification coefficient on the gain rate in the resonant layer model for a given dissipative damping $\gamma_d = 10^{12} \text{s}^{-1}$. For the black curve $\gamma_{rn} = 0$, for the red curve $\gamma_{rn} = 10^{10} \text{s}^{-1}$, for the blue curve $\gamma_{rn} = 10^{11} \text{s}^{-1}$, and for the green curve $\gamma_{rn} = 10^{12} \text{s}^{-1}$.

required. The lasing is reached when the gain also counterbalances the radiative damping of the plasmon mode.

3. To reach the laser regime, the plasmon modes with stronger radiative damping require a larger gain.

4. The plasmon resonance HWHM Δf (in Hz) is determined by the equation $2\pi \Delta f = \gamma_d + \gamma_{rn} + \gamma_g$. The maximum of absorbance is reached when the equality $\gamma_d + \gamma_g = \gamma_{rn}$ is fulfilled, and the resonance HWHM $\Delta f_{\text{max}A}$ in this case is determined by the expression $2\pi \Delta f_{\text{max}A} = 2(\gamma_d + \gamma_g) = 2\gamma_{rn}$. At frequencies where the gain counterbalances the dissipative losses $\gamma_d = -\gamma_g$ the resonance HWHM Δf is fully determined by the radiative damping as $2\pi \Delta f = \gamma_{rn}$. The structure with $\gamma_d = -\gamma_g$ is totally reflective ($A_n = T_n = 0$, $R_n = 1$) at the plasmon resonance.

These implications allow us to conclude that, for achieving the plasmon lasing, it is efficient to use weak plasmon modes, i.e., modes with small radiative damping.

Radiative damping can be associated with the net dipole moment of the plasmon mode, since it is the dipole moment that accounts for coupling the plasmon mode with the incident THz wave.

In this work we investigate weak plasmon modes in a periodical two-layer graphene structure and in a spatially asymmetric grating-gate graphene structures.

III. GAIN IN A PUMPED GRAPHENE

The electromagnetic response of graphene to an acting electric field is described by the conductivity function with

inverted charge-carrier distribution [36]

$$\begin{aligned} \sigma(\omega) &= \frac{e^2 2k_B T \tau}{\pi \hbar^2 (1 - i\omega\tau)} \ln \left[1 + \exp \left(\frac{\mathcal{E}_F}{k_B T} \right) \right] \\ &+ \frac{e^2}{4\hbar} \tanh \left(\frac{\hbar\omega - 2\mathcal{E}_F}{4k_B T} \right) \\ &+ i \frac{e^2 \omega}{\pi} \int_0^\infty \frac{G(\xi) - G(\hbar\omega/2)}{(\hbar\omega)^2 - 4\xi^2} d\xi, \\ G(\xi) &= \frac{\sinh(\xi/k_B T)}{\cosh(\xi/k_B T) + \cosh(\mathcal{E}_F/k_B T)}, \end{aligned}$$

where \mathcal{E}_F is the quasi-Fermi energy in graphene ($\mathcal{E}_F > 0$ for electrons and $-\mathcal{E}_F$ for holes), $k_B T$ is the thermal energy of charge carriers in graphene, and τ is the momentum relaxation time of charge carriers in graphene. Energy exchange between the incident wave and charge carriers in active graphene is described by the relation

$$\begin{aligned} Q &= \frac{1}{2} \int_{-L/2}^{L/2} \text{Re} [j_\omega^* E_{x,\omega}] dx \\ &= \frac{1}{2} \int_{-L/2}^{L/2} \text{Re} [\sigma(\omega)] |E_{x,\omega}|^2 dx, \end{aligned}$$

where j_ω is the current density in graphene, $E_{x,\omega}$ is the in-plane component of electric field in graphene, L is the length of a period of the graphene structure. Here, the real part of conductivity $\text{Re} [\sigma(\omega)] > 0$ corresponds to absorption of electromagnetic energy and $\text{Re} [\sigma(\omega)] < 0$ corresponds to amplification. The real part of the conductivity can be written as

$$\text{Re} [\sigma(\omega)] = \frac{e^2 2k_B T \ln [1 + \exp(\mathcal{E}_F/k_B T)]}{\hbar^2 \pi (\omega^2 + \tilde{\gamma}_d^2)} (\tilde{\gamma}_d + \tilde{\gamma}_g),$$

where value

$$\tilde{\gamma}_g = \frac{(\omega^2 + \tilde{\gamma}_d^2) \pi \hbar}{8k_B T \ln [1 + \exp(\mathcal{E}_F/k_B T)]} \tanh \left(\frac{\hbar\omega - 2\mathcal{E}_F}{4k_B T} \right) \quad (4)$$

describes the gain in graphene, and $\tilde{\gamma}_d = 1/\tau$ is the graphene dissipative damping. Plasmon damping rate is equal to a half of the graphene damping rate $\gamma_d = \tilde{\gamma}_d/2$ [30], and, by analogy, plasmon gain rate in active graphene is equal to a half of the graphene gain rate $\gamma_g = \tilde{\gamma}_g/2$. In contrast to the conductivity, which describes the collective response of all charged particles in graphene, the value of gain rate γ_g as well as the dissipative damping rate γ_d are attributed to the dynamics of an average particle. As a result, with an increase of the density of charged particles (and quasi-Fermi energy), the value of the gain γ_g , Eq. (4), decreases (Fig. 2), since the energy released during

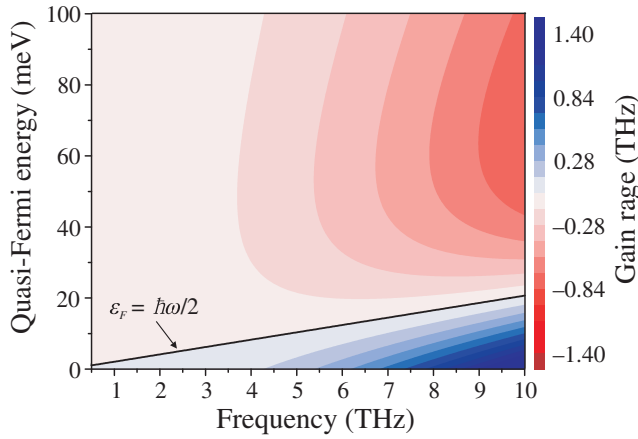


FIG. 2. Dependence of the plasmon gain rate γ_g for active graphene on frequency and quasi-Fermi energy at $T = 300$ K and $\tau = 1$ ps. The black line corresponds to the switch between lossy and gain regimes.

radiative recombination is distributed among all oscillating charged particles. An increase in gain with frequency occurs due to an increase in the portion of the energy radiated during radiative recombination process, distributed among the charge carriers participating in the oscillations (Fig. 2). And the gain increases with the dissipative damping rate γ_d because rapid relaxation of excited carriers to the equilibrium inverted distribution, which increases the number of possible radiative transitions in graphene.

IV. THE PLASMON AMPLIFICATION SPECTRA

In this work, we investigate the achievement of the plasmon lasing regime at weak plasmon modes. The term “weak” is used for describing the efficiency of the excitation of plasmon modes and can be numerically related to their small radiative damping. The main feature of the weak plasmon modes is their small net dipole moment, and this property depends on the geometric symmetry of the structure. The weak plasmon modes can be of two different types: antiphase oscillations in multilayered structures and modes with even spatial distribution of the oscillating charge with respect to the center of the stripe. In this work, two types of weak plasmon modes are considered for two periodic plasmonic structures based on graphene.

In periodic structure no. 1, the unit cell consists of two graphene stripes located one above the other and separated by a barrier dielectric layer (Fig. 3). The stripes can be of different widths, with the center of the upper stripe located above the center of the lower strip. An electromagnetic wave incident normally onto the structure with electric field polarization across the graphene stripes can excite plasmons in the structure. The strong plasmon modes in such a structure are the “optical” plasmons [37] with conventional square-root dispersion relation, which

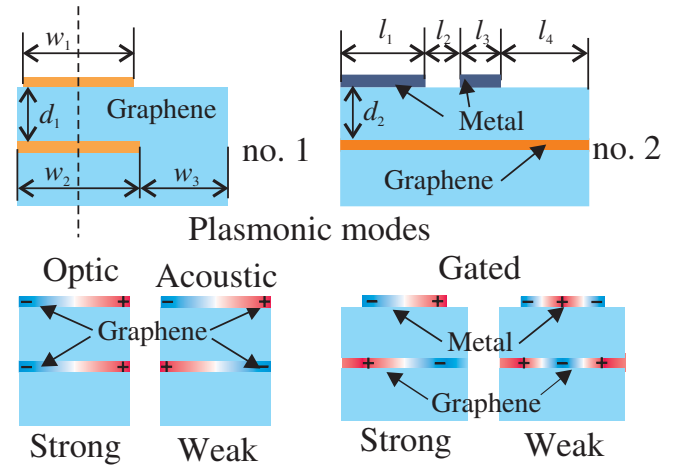


FIG. 3. Schematic view of the unit cells of periodic graphene structures no. 1 and no. 2. The basic geometrical parameters are shown at the top of the picture, schematic instant charge distribution for strong and weak plasmon modes are shown in the bottom of the picture.

are characterized by in-phase oscillation of charges in graphene layers located one above the other. The weak modes here are the two-layer “acoustic” plasmon modes [38,39]. In such “acoustic” plasmon modes, the antiphase oscillations of charges in parallel graphene layers occur. If the widths of the upper and lower stripes are equal, then there is almost complete screening of oscillating charges in different parallel stripes by each other in weak plasmon mode. Only a small phase incursion of the incident THz wave passing through the structure slightly deteriorates the antiphase oscillations in parallel graphene stripes and allows for weak excitation of “acoustic” plasmons.

A periodic graphene structure with a dual metal grating gate and an asymmetric unit cell (structure no. 2) (Fig. 3) is also considered. In such a structure, two metal subgrating gates are situated in the same plane and have electrodes of different widths. The strong plasmon modes in this structure are the typical gated plasmons [33], which have antisymmetric spatial charge distribution in graphene with respect to the center of the gate electrode. The weak gated “nonradiative” plasmon mode here has an even spatial distribution of the oscillating charge in graphene under the gate electrode with respect to the center of the gate electrode [33]. Such a mode cannot be excited in a structure no. 2 with a symmetric unit cell, since the total dipole moment of such a plasmon mode is zero in that case.

Investigations of plasmon modes in structures no. 1 and no. 2 are carried out using electromagnetic algorithms developed by the authors based on the forming and solving an integral equations for the oscillating currents in conducting elements of the periodic structures (similar algorithms are published in Refs. [33,34]). The response

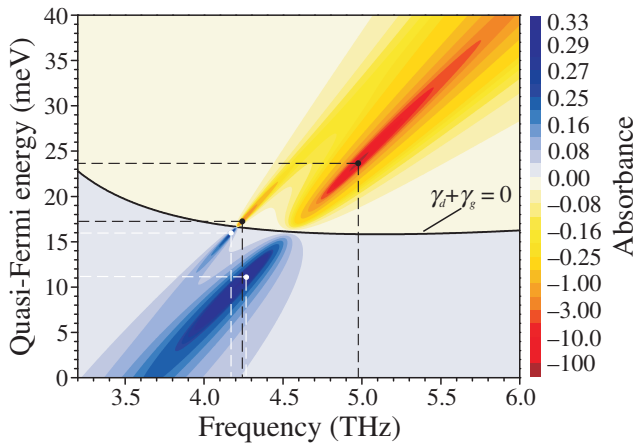


FIG. 4. Dependence of absorbance for structure no. 1 on frequency and quasi-Fermi energy. “Acoustic” and “optical” plasmon modes are shown (from left to right on frequency axes, correspondingly). The laser points of plasmon modes are denoted by the black dots. The points of maximum absorbance are shown by white dots. The black curve shows the total reflectance line for $\gamma_d = -\gamma_g$. Parameters are $w_1 = w_2 = 0.5 \mu\text{m}$, $w_3 = 0.25 \mu\text{m}$, $d = 30 \text{ nm}$.

of graphene to a THz field in the electromagnetic approach is described by conductivity (4).

For structure no. 1, the plasmon amplification spectra are investigated (Fig. 4) for two plasmon modes (“acoustic” and “optical”). In a structure with equal widths of the upper and lower graphene stripes, the “acoustic” mode has a small total dipole moment since, for a small distance between the graphene stripes compared to the THz wavelength, the antiphase charges in the upper and lower graphene stripes almost completely screen each other (Fig. 3). Due to this property, the “acoustic” plasmon mode is weakly excited, which corresponds to its small radiative damping. Figure 4 shows the evolution of plasmon modes as a function of the quasi-Fermi energy, which is determined by graphene pumping. The weak “acoustic” mode is excited in structure no. 1 near the total reflectance line ($\text{Re}[\sigma(\omega)] = 0$). In such a structure with equal graphene stripe widths ($w_1 = w_2$), the radiative damping reaches minimum values for the “acoustic” mode, but does not vanish, since the charges in different stripes planes do not oscillate exactly in antiphase.

We calculate the radiative damping of the “optical” [Fig. 5(a)] and “acoustic” [Fig. 5(b)] plasmon modes in structure no. 1 as the difference between the HWHM and the gain rate and dissipative damping values, $\gamma_m = 2\pi\Delta f - \gamma_d - \gamma_g$, where γ_g is calculated using Eq. (4). This is confirmed by the fact that the gain calculated from the width of the plasmon resonance at the particular points of the maximum absorption of the structure and the total reflectance of the structure completely coincides with the gain calculated using Eq. (4).

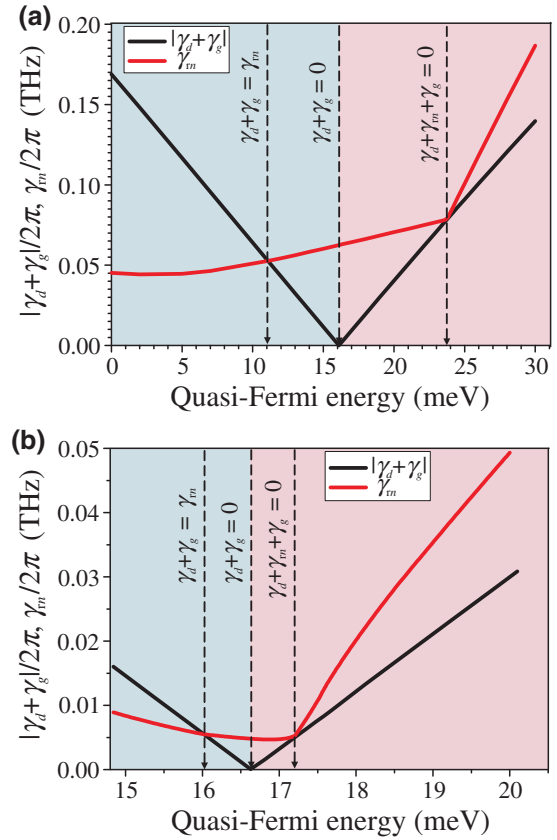


FIG. 5. Evolution of radiative damping of “optical” (a) and “acoustic” (b) plasmon modes with increasing quasi-Fermi energy in graphene for structure no. 1. Figures (a) and (b) are calculated along the plasmon resonance lobes from Fig. 4.

Each plasmon mode passes through several particular points with increasing pumping (Fig. 4). At the *first* point, the absorption coefficient reaches its maximum positive value when equality $\gamma_d + \gamma_g = \gamma_m$ is satisfied (Fig. 5). Since under these conditions the radiative damping occupies exactly half of the HWHM, the gain achieved in this resonance can be easily calculated using the relation $\gamma_g = \pi\Delta f_{\text{max}A} - \gamma_d$.

The *second* particular point is passed when the real part of the graphene conductivity is zero; in this case, the absorbance of the structure is zero, and the reflection coefficient of the structure reaches unity. Moreover, the HWHM is equal to the radiative damping, and the gain is exactly equal to the dissipative damping $\gamma_d + \gamma_g = 0$ (Fig. 5).

Lasing regime is reached at the *third* particular point ($A \rightarrow -\infty$, $R + T \rightarrow \infty$, $\Delta f \rightarrow 0$) when the condition $\gamma_d + \gamma_m = -\gamma_g$ is fulfilled (Fig. 5), when the gain fully counterbalances the dissipative and radiative dampings.

We find out that the radiative damping of the “acoustic” mode is an order of magnitude smaller than the radiative damping of the “optical” mode (Fig. 5). This means that in a weak “acoustic” plasmon mode, the threshold for the

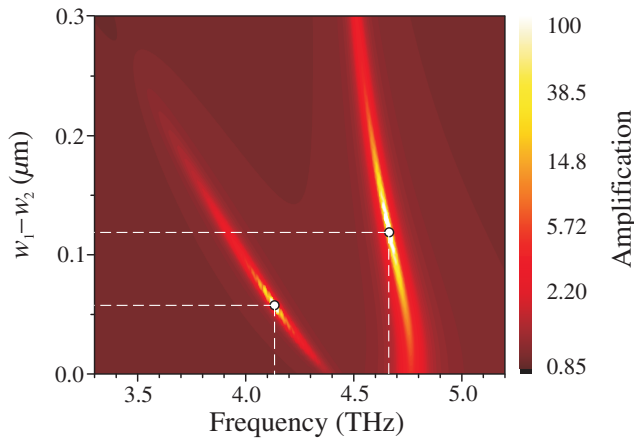


FIG. 6. Dependence of amplification for structure no. 1 on frequency and difference of the graphene stripe widths $w_2 - w_1$. “Acoustic” and “optical” plasmon modes are shown (from left to right on frequency axes, correspondingly). The laser points of plasmon modes are shown by circles. Parameters are $w_1 = 0.5 \mu\text{m}$, $w_3 = 0.25 \mu\text{m}$, $d_1 = 30 \text{ nm}$, $\mathcal{E}_F = 20 \text{ meV}$.

lasing can be significantly reduced, which can be seen in Figs. 4 and 5. It can also be seen that the radiative-damping curve changes the slope at the quasi-Fermi energies greater than necessary for the appearance of the laser regime. Such behavior of the radiative damping can be explained by a change in the fraction of charge carriers participating in the plasma oscillation $N_s \beta_n^2$.

For structure no. 1, the plasmon amplification spectra are calculated (Fig. 6) for two plasmon modes (“acoustic” and “optical”) depending on the difference of graphene-stripe widths $w_2 - w_1$ with increasing width of the lower graphene stripe. The unscreened regions of the lower graphene layer lead to incomplete screening of the charges in the graphene stripes and, hence, lead to an increase in the radiative damping of the weak plasmon mode. When the balance $\gamma_d + \gamma_m = -\gamma_g$ is achieved by adjusting the radiative damping of the “acoustic” plasmon mode, a laser regime appears (Fig. 6). Figure 6 is calculated in such a way that the laser regimes are achieved at both weak “acoustic” and strong “optical” plasmon modes.

Weak modes in a graphene structure no. 2 with a dual-grating gate are excited in spatially asymmetric structures (Fig. 7). For structures with different widths of the subgrating fingers in the unit cell, the asymmetry can be described by the value of the asymmetry coefficient $K_{\text{no.2}} = 1 - l_2/l_4$, where $K_{\text{no.2}} = 0$ corresponds to a symmetric structure. With a dual grating gate located close to isotropic graphene in structure no. 2, the gated plasmon modes can be excited with wave vectors in the inverse multiples of the widths of the gate subgrating fingers $q_p = \pi p/l_{1,3}$, with p being a positive integer. The plasmon modes with wave

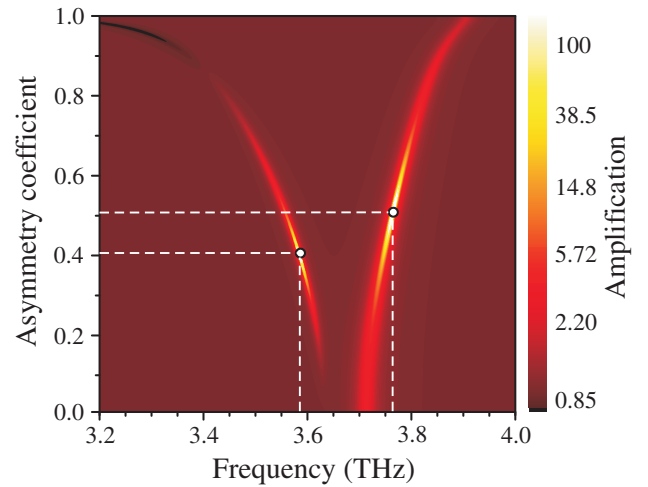


FIG. 7. Dependence of amplification for structure no. 2 on frequency and asymmetry coefficient $K_{\#2}$. “Radiative” and “non-radiative” plasmon modes are shown. Parameters are $l_1 = 0.22 \mu\text{m}$, $l_3 = 0.15 \mu\text{m}$, $l_2 + l_4 = 0.190 \mu\text{m}$, $d_2 = 15 \text{ nm}$, $\mathcal{E}_F = 20.5 \text{ meV}$.

vectors q_p for p being an even number are weak “non-radiative” modes, which cannot be excited in the case of $K_{\text{no.2}} = 0$ (Fig. 7).

By choosing a suitable asymmetry coefficient of structure no. 2, the radiation damping of the weak plasmon mode can be changed so as to satisfy the condition of lasing at the weak mode (Fig. 7, $K_{\text{no.2}} = 0.4$).

We investigate the change in radiative damping upon reaching the laser regime for a weak “nonradiative” plasmon mode depending on the width of the gate electrode (i.e., the width of the plasmon resonator in which the weak plasmon mode is excited) (Fig. 8). The separation of the resonance of the weak plasmon mode from the strong mode (excited under the gate l_3) made it possible to further reduce the radiative damping of the weak mode by an order of magnitude (Fig. 8) to values of 0.5 GHz (the damping rates, expressed in Hz, are obtained by their dividing by 2π).

The difference by 2 orders of magnitude in the radiative damping of strong and weak plasmon modes makes it possible to lower the pumping strength of graphene practically to the level of compensation of the dissipative losses for reaching the laser regime for the weak plasmon mode.

The radiative damping of the weak plasmon modes are $\gamma_m \sim 5 \text{ GHz}$ for structure no. 1 and $\gamma_m \sim 0.5 \text{ GHz}$ for structure no. 2. Whereas, for a strong “radiative” plasmon mode the gain should overcome for a rather greater radiative damping (about 0.08 THz), which is comparable with plasmon dissipative damping 0.079 THz for $\tau = 1 \text{ ps}$ being used for the calculations.

Since the wave vector of plasmons is determined by the geometric parameters of the resonator as $\pi p/w_{1,2}$ and

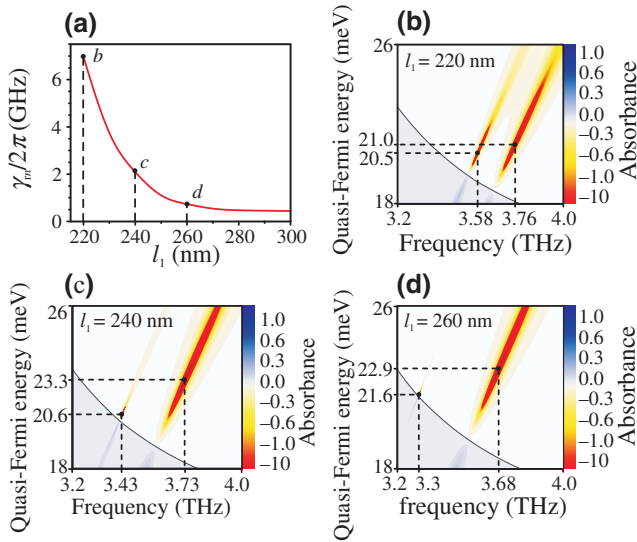


FIG. 8. (a) The radiative damping versus the gate width l_1 corresponding to the laser regimes of the weak “nonradiative” mode for structure no. 2. (b)–(d) Dependence of absorbance for structure no. 2 on frequency and quasi-Fermi energy for different widths l_1 : (b) $l_1 = 0.22 \mu\text{m}$, (c) $l_1 = 0.24 \mu\text{m}$, and (d) $l_1 = 0.26 \mu\text{m}$. “Radiative” and “nonradiative” gated plasmon modes are shown. Black curves in (b)–(d) show the total reflectance line for $\gamma_d = -\gamma_g$. Parameters of (b)–(d) are $l_3 = 0.15 \mu\text{m}$, $l_2 = 70 \text{ nm}$, $l_4 = 120 \text{ nm}$, $d_2 = 15 \text{ nm}$.

$\pi p/l_{1,3}$, it is possible to tune the frequencies of weak plasmon modes in structures no. 1 and no. 2 to a required lasing frequency.

Structures no. 1 and no. 2 are open structures for electromagnetic wave, as a result of which the excited or amplified plasmons in them are radiated into outgoing electromagnetic waves. The value of radiative damping of the plasmon mode controls the level of outgoing electromagnetic waves and Q factor of the plasmon resonance. The narrow width of amplification region on frequency scale for weak plasmon modes allows for single-mode operation.

V. CONCLUSIONS

The gain rates of strong and weak plasmon modes in graphene structures are calculated using conductivity function. The radiative damping of plasmon modes in graphene structures are calculated utilizing a strict electromagnetic approach and using the linear oscillator model for plasmons, and calculated gain rate. It is found that in asymmetric structures, the lasing regime for weak plasmon modes is possible: for the “acoustic” two-layer plasmon and for “nonradiative” gated plasmon. The advantage of using the weak modes for lasing is that they have weak radiative losses, which significantly lowers the lasing threshold. The

possibility of changing the frequency and radiative damping of weak modes by the structure geometry can be used to tune the regime of laser generation of plasmons.

ACKNOWLEDGMENTS

The work is carried out within the framework of a state task.

- [1] T. Otsuji and M. Shur, Terahertz plasmonics: Good results and great expectations, *IEEE Microw. Mag.* **15**, 46 (2014).
- [2] K. S. Novoselov, V. I. Falko, L. Colombo, P. R. Gellert, M. G. Schwab, and K. Kim, A roadmap for graphene, *Nature* **490**, 192 (2012).
- [3] S. Huang, C. Song, G. Zhang, and H. Yan, Graphene plasmonics: Physics and potential applications, *Nanophotonics* **6**, 1191 (2017).
- [4] Y. Fan, F. Zhang, H. Wu, Q. Fu, N. Shen, C. Soukoulis, Q. Zhao, Z. Wei, and H. Li, Graphene plasmonics: A platform for 2D optics, *Adv. Opt. Mater.* **7**, 1800537 (2019).
- [5] J. Chen, M. Badioli, P. Alonso-González, S. Thongratanasiri, F. Huth, J. Osmond, M. Spasenovi, A. Centeno, A. Pesquera, P. Godignon, A. Z. Elorza, N. Camara, F. J. G. D. Abajo, R. Hillenbrand, and F. H. L. Koppens, Optical nano-imaging of gate-tunable graphene plasmons, *Nature* **487**, 77 (2012).
- [6] M. Orlita, C. Faugeras, P. Plochocka, P. Neugebauer, G. Martinez, D. K. Maude, A.-L. Barra, M. Sprinkle, C. Berger, W. A. de Heer, and M. Potemski, Approaching the Dirac Point in High-Mobility Multilayer Epitaxial Graphene, *Phys. Rev. Lett.* **101**, 267601 (2008).
- [7] M. B. Lundberg, Y. Gao, A. Woessner, C. Tan, P. Alonso-González, K. Watanabe, T. Taniguchi, J. Hone, R. Hillenbrand, and F. H. L. Koppens, Thermoelectric detection and imaging of propagating graphene plasmons, *Nat. Mater.* **16**, 204 (2016).
- [8] D. A. Bandurin, D. Svintsov, I. Gayduchenko, S. G. Xu, A. Principi, M. Moskotin, I. Tretyakov, D. Yagodkin, S. Zhukov, T. Taniguchi, K. Watanabe, I. V. Grigorieva, M. Polini, G. N. Goltsman, A. K. Geim, and G. Fedorov, Resonant terahertz detection using graphene plasmons, *Nat. Commun.* **9**, 5392 (2018).
- [9] J. R. Williams, L. DiCarlo, and C. M. Marcus, Quantum hall effect in a gate-controlled p - n junction of graphene, *Science* **317**, 638 (2007).
- [10] T. Lohmann, K. von Klitzing, and J. H. Smet, Four-terminal magneto-transport in graphene p - n junctions created by spatially selective doping, *Nano. Lett.* **9**, 1973 (2009).
- [11] P. Olbrich, J. Kamann, M. König, J. Munzert, L. Tutsch, J. Eroms, D. Weiss, M. H. Liu, L. E. Golub, E. L. Ivchenko, V. V. Popov, D. V. Fateev, K. V. Mashinsky, F. Fromm, T. Seyller, and S. D. Ganiev, Terahertz ratchet effects in graphene with a lateral superlattice, *Phys. Rev. B* **93**, 075422 (2016).
- [12] J. A. Delgado-Notario, V. Clericó, E. Díez, J. E. Velázquez-Pérez, T. Taniguchi, K. Watanabe, T. Otsuji, and Y. M. Meziani, Asymmetric dual-grating gates graphene fet for

- detection of terahertz radiations, *APL Photonics* **5**, 066102 (2020).
- [13] A. A. Dubinov, V. Y. Aleshkin, V. Mitin, T. Otsuji, and V. Ryzhii, Terahertz surface plasmons in optically pumped graphene structures, *J. Phys.: Condens. Matter* **23**, 145302 (2011).
- [14] V. V. Popov, O. V. Polischuk, A. R. Davoyan, V. Ryzhii, T. Otsuji, and M. S. Shur, Plasmonic terahertz lasing in an array of graphene nanocavities, *Phys. Rev. B* **86**, 195437 (2012).
- [15] T. Watanabe, T. Fukushima, Y. Yabe, S. A. B. Tombet, A. Satou, A. A. Dubinov, V. Y. Aleshkin, V. Mitin, V. Ryzhii, and T. Otsuji, The gain enhancement effect of surface plasmon polaritons on terahertz stimulated emission in optically pumped monolayer graphene, *New J. Phys.* **15**, 075003 (2013).
- [16] V. Ryzhii, M. Ryzhii, V. Mitin, and T. Otsuji, Toward the creation of terahertz graphene injection laser, *J. Appl. Phys.* **110**, 094503 (2011).
- [17] V. Ryzhii, I. Semenikhin, M. Ryzhii, D. Svintsov, V. Vyurkov, A. Satou, and T. Otsuji, Double injection in graphene *p-i-n* structures, *J. Appl. Phys.* **113**, 244505 (2013).
- [18] R. Jago, T. Winzer, A. Knorr, and E. Malić, Graphene as gain medium for broadband lasers, *Phys. Rev. B* **92**, 085407 (2015).
- [19] D. Yadav, G. Tamamushi, T. Watanabe, J. Mitsushio, Y. Tobah, K. Sugawara, A. A. Dubinov, A. Satou, M. Ryzhii, V. Ryzhii, and T. Otsuji, Terahertz light-emitting graphene-channel transistor toward single-mode lasing, *Nanophotonics* **7**, 741 (2018).
- [20] G. Alymov, V. Vyurkov, V. Ryzhii, A. Satou, and D. Svintsov, Auger recombination in dirac materials: A tangle of many-body effects, *Phys. Rev. B* **97**, 205411 (2018).
- [21] P. Huang, E. Riccardi, S. Messelot, H. Graef, F. Valmorra, J. Tignon, T. Taniguchi, K. Watanabe, S. Dhillon, B. Plaças, R. Ferreira, and J. Mangeney, Ultra-long carrier lifetime in neutral graphene-hBN van der Waals heterostructures under mid-infrared illumination, *Nat. Commun.* **11**, 863 (2020).
- [22] M. Morozov, V. G. Leiman, V. V. Popov, V. Mitin, M. S. Shur, V. E. Karasik, M. Ryzhii, T. Otsuji, and V. Ryzhii, Optical pumping in graphene-based terahertz/far-infrared superluminescent and laser heterostructures with graded-gap black-P_xAs_{1-x} absorbing-cooling layers, *Opt. Eng.* **59**, 061606 (2019).
- [23] M. Y. Morozov, V. V. Popov, M. Ryzhii, V. G. Leiman, V. Mitin, M. S. Shur, T. Otsuji, and V. Ryzhii, Optical pumping through a black-as absorbing-cooling layer in graphene-based heterostructure: Thermo-diffusion model, *Opt. Material Express* **9**, 4061 (2019).
- [24] O. V. Polischuk, D. V. Fateev, T. Otsuji, and V. V. Popov, Plasmonic amplification of terahertz radiation in a periodic graphene structure with the carrier injection, *Appl. Phys. Lett.* **111**, 081110 (2017).
- [25] D. Svintsov, Emission of plasmons by drifting dirac electrons: A hallmark of hydrodynamic transport, *Phys. Rev. B* **100**, 195428 (2019).
- [26] D. A. Bandurin, I. Torre, R. K. Kumar, M. B. Shalom, A. Tomadin, A. Principi, G. H. Auton, E. Khestanova, K. S. Novoselov, I. V. Grigorieva, L. A. Ponomarenko, A. K. Geim, and M. Polini, Negative local resistance caused by viscous electron backflow in graphene, *Science* **351**, 1055 (2016).
- [27] R. K. Kumar, D. A. Bandurin, F. M. D. Pellegrino, Y. Cao, A. Principi, H. Guo, G. H. Auton, M. B. Shalom, L. A. Ponomarenko, G. Falkovich, K. Watanabe, T. Taniguchi, I. V. Grigorieva, L. S. Levitov, M. Polini, and A. K. Geim, Superballistic flow of viscous electron fluid through graphene constrictions, *Nat. Phys.* **13**, 1182 (2017).
- [28] D. Svintsov, Hydrodynamic-to-ballistic crossover in dirac materials, *Phys. Rev. B* **97**, 121405(R) (2018).
- [29] V. V. Popov, M. S. Shur, G. M. Tsymbalov, and D. V. Fateev, Higher-order plasmon resonances in gan-based field-effect transistor arrays, *Int. J. High Speed Electron. Syst.* **17**, 557 (2007).
- [30] V. V. Popov, O. V. Polischuk, T. V. Teperik, X. G. Peralta, S. J. Allen, N. J. M. Horing, and M. C. Wanke, Absorption of terahertz radiation by plasmon modes in a grid-gated double-quantum-well field-effect transistor, *J. Appl. Phys.* **94**, 3556 (2003).
- [31] O. V. Polischuk, V. V. Popov, and T. Otsuji, Superradiant amplification of terahertz radiation by plasmons in inverted graphene with a planar distributed bragg resonator, *Semiconductors* **49**, 1468 (2015).
- [32] V. V. Popov, D. V. Fateev, E. L. Ivchenko, and S. D. Ganichev, Noncentrosymmetric plasmon modes and giant terahertz photocurrent in a two-dimensional plasmonic crystal, *Phys. Rev. B* **91**, 235436 (2015).
- [33] D. V. Fateev, K. V. Mashinsky, O. V. Polischuk, and V. V. Popov, Excitation of Propagating Plasmons in a Periodic Graphene Structure by Incident Terahertz Waves, *Phys. Rev. Appl.* **11**, 064002 (2019).
- [34] I. M. Moiseenko, V. V. Popov, and D. V. Fateev, Amplified propagating plasmon in asymmetrical graphene periodic structure, *J. Phys. Commun.* **4**, 071001 (2020).
- [35] D. Svintsov, V. Vyurkov, V. Ryzhii, and T. Otsuji, Hydrodynamic electron transport and nonlinear waves in graphene, *Phys. Rev. B* **88**, 245444 (2013).
- [36] V. Ryzhii and M. Ryzhii, Negative dynamic conductivity of graphene with optical pumping, *J. Appl. Phys.* **101**, 083114 (2007).
- [37] A. V. Chaplik, Absorption and emission of electromagnetic waves by two-dimensional plasmons, *Surf. Sci. Rep.* **5**, 289 (1985).
- [38] T. Stauber and G. Gómez-Santos, Plasmons in layered structures including graphene, *New J. Phys.* **14**, 105018 (2012).
- [39] P. Alonso-González, A. Y. Nikitin, Y. Gao, A. Woessner, M. B. Lundeberg, A. Principi, N. Forcellini, W. Yan, S. Vélez, A. J. Huber, K. Watanabe, T. Taniguchi, F. Casanova, L. E. Hueso, M. Polini, J. Hone, F. H. L. Koppens, and R. Hillenbrand, Acoustic terahertz graphene plasmons revealed by photocurrent nanoscopy, *Nat. Nanotechnol.* **12**, 31 (2017).